Hindawi
Advances in Materials Science and Engineering
Volume 2019, Article ID 7079819, 15 pages
https://doi.org/10.1155/2019/7079819

Research Article

Fretting Wear Behavior and Damage Mechanisms of Inconel X-750 Alloy in Dry Contacts

Ibrohim A. Rustamov[1], **Ozoda Sh. Sabirova**[2], **Zixi Wang**[1], **and Yuming Wang**[1]

[1]*State Key Laboratory of Tribology, Tsinghua University, Beijing 100084, China*
[2]*Department of Mechanical Engineering, Tashkent State Technical University, Tashkent 100095, Uzbekistan*

Correspondence should be addressed to Zixi Wang; zxwang@mail.tsinghua.edu.cn

Received 10 November 2018; Revised 19 January 2019; Accepted 12 February 2019; Published 4 March 2019

Academic Editor: Hongtao Zhu

Tribological behavior of the Inconel X-750 alloy disk subjected to fretting against the GCr15 steel ball was investigated in an ambient laboratory air with relative humidity of 55–65%. A high-frequency oscillating Optimol SRV 4 tribometer was employed to execute dry fretting tests in the partial and gross slip regimes under constant 100 N normal load. Tests were carried out for 10, 30, and 90 minutes, and the friction forces vs. displacement amplitudes were monitored during the test duration. Posttest examinations were conducted utilizing advanced tools such as 3D optical surface profiler, scanning electron microscopy (SEM), and energy dispersive X-ray spectroscopy (EDX). The main objective was to obtain wear scar evolutions, frictional properties, and degradation mechanisms under the different running conditions over time. It was found that fretting wear behaviors of friction pairs were strongly influenced by fretting regimes. Degradation evolutions were greatly influenced by fretting time during partial slip regimes, i.e., evolving from asperity deformation and slight damage to the fatigue crack and material transfer. However, the combination of adhesive, abrasive, delamination, and wear oxidation mechanisms was repeated during the entire gross slip fretting process.

1. Introduction

The definition of fretting is given as a complex wear phenomenon between contacting surfaces subjected to relative vibratory movements with a small amplitude at high frequencies [1], as other authors offered the definition of *"fretting is a relative cyclic motion between two surfaces, having a nonuniform distribution of local relative displacement at their contact"* [2]. Based on the published experimental data, fretting regimes are broken into three different sliding forms, namely, stick, partial slip, and gross slip which controls the contact interface as long as the fretting process makes the transition to the reciprocating motion [3]. The distribution of local relative displacement refers to the alterations of the sliding conditions over the contact interface, i.e., zero relative displacement during stick, small slip in the periphery, and zero displacement in the sticking portion during partial slip, and more uniformly distributed relative displacement in the entire contact during gross slip. Furthermore, taking the imposed displacement into account, fretting conditions between two convex pairs or ball-on-flat contacts were described by Mindlin's elastic model in relation to two shear models [4]. In small displacements, the corresponding tangential force, F_t, is smaller than the critical total sliding shear force, and as a result, contact is in partial slip with the central stick region and a ring-shaped annulus where sliding occurs. As the displacement amplitude increases, the tangential force reaches the critical total sliding value; therefore, the stick region in the contact center disappears gradually and gross slip occupies the whole contact interface. This trend can be described by the relation of $F_t > \mu P$, where P is the applied normal force and μ is the friction coefficient.

Fretting maps which are proposed by Vingsbo and Söderberg [3] and developed by Zhou and Vincent [5] are used nowadays to represent the fretting regimes and

damages based on the normal load and the displacement amplitude (Figure 1(a)). The relationship between tangential force and imposed displacement amplitude, the so-called *"fretting loop,"* was closed, elliptical and parallelogram during stick, partial slip, and gross slip conditions, respectively. Besides, Varenberg et al. [2] introduced a new terminology *"slip index"* to identify all the different fretting regimes. The dimensionless slip index is obtained from a fretting loop which is shown schematically in Figure 1(b). The slip amplitude, A_s, is a function of all the independent governing parameters, such as the imposed displacement amplitude, A_d, the normal load, P, and the elastic slope of fretting loop, S_c. According to their study, fretting exists when $\delta < 10$. Partial slip is present in δ values between 05 and 0.6, while gross slip prevails in the range of 0.8 and 10. Beyond this range, reciprocal sliding occurs ($\delta > 11$). The enclosed area by fretting loop corresponds to the dissipated energy, E_d, which is related to the wear produced during a particular fretting time [6, 7].

The fretting wear behavior of materials is also a very complicated phenomenon in which different damage mechanisms (adhesion, plastic deformation, abrasion, fatigue crack, delamination, and oxidation) and factors (contact geometries, material properties, and environmental conditions) are involved [8, 9]. Depending on the running conditions, the material responses can be deformed asperity adhesion in the stick, crack initiation and propagation in the partial slip regime (PSR) and loss of material by wear in the gross slip regime (GSR) [10, 11]. The material removal is usually very slow process in well-designed tribological systems; however, it is very steady and continuous. Contact surfaces subjected to fretting have a specific appearance with red-brown patches on ferrous metals as a result of lapping by metallic oxide debris [12]. It is also noticed that the wear of surfaces that undergo fretting is strongly affected by the environment, i.e., the amount of fretting wear in humid air is substantially greater than that observed in dry air [13].

In the last decade, most of the fretting wear experiments have been conducted on the nickel-based nuclear engineering materials, such as Inconel 600, 690, and 690 TT alloys which are known for their corrosion and oxidation resistance in the elevated temperatures [14–19]. The effects of different fretting parameters (e.g., sliding amplitude, normal load, and temperature) and material properties (e.g., heat treatment, precipitated carbides, grain size, hardness, and microstructural characterizations) were investigated in their study to evaluate different degradation mechanisms and fretting behaviors. As far as these factors make fretting a system property, the complexity of the contact interactions should be clarified by precise alignments of the specimens and proper laboratory environment. In this work, suitable laboratory experiment was set to investigate the tribological properties of Inconel X-750 alloy under both partial and gross slip conditions in dry ball-on-flat contact configuration. Inconel X-750 is a precipitation-hardenable nickel-chromium based super alloy, where it is widely used in gas turbines, pressure vessels, rocket engines, nuclear reactors, tooling, and aircraft structures [20]. Its outstanding relaxation resistance is beneficial for high-temperature springs and bolts. Besides, it has good resistance to corrosion and oxidation, as well as high tensile and creep-rupture properties at elevated temperatures after a suitable heat treatment [21]. Limited experimental works are performed concerning about its mechanical properties in different temperature environments [22], but no literature includes the fretting wear behaviors of Inconel X-750 alloy. Thus, the specific objectives of the present study would contribute to a better knowledge of the tribological nature and surface degradation evolutions of Inconel X-750 alloy during fretting wear process.

2. Experimental Setup

Ball-on-flat fretting experiments were run at room temperature of 20–25°C using the SRV 4 (Optimol Instruments, Germany) high-frequency oscillation system with 50–60% air humidity in dry condition. The test rig is equipped with a soundproof chamber, integrated electronic measurements, load cell, oscillating rods, and other modules to control fretting parameters as shown in Figure 2. The lower Inconel X-750 (solution annealed at 980°C for 2 h) disk specimen with 24 mm diameter × 7.8 mm height was fixed by clamps and subjected to the fretting by upper oscillating GCr15 (Chinese GB 308–89) steel ball with diameter of 10 mm and roughness of 0.025 μm (Ra). Table 1 shows the chemical compositions for both of the friction materials. Modulus of elasticity and Poisson's ratio are 214 GPa and 0.29 for X-750 alloy, and 210 GPa and 0.3 for GCr15 ball, respectively. Vickers hardness tests were performed by Qness (Austria) with the 20 μm diameter pyramidal diamond tip, and 296 HV was obtained for Inconel X-750 alloy, while 758 HV measured for GCr15 ball. Lower specimens were machined according to the test rig specifications and grounded with waterproof SiC abrasive papers (grain size 5 μm), subsequently polished with water based polycrystalline diamond paste (particle size 1 μm) to have a mirror finish. Prior to the test, ball and disk specimens were cleaned in an ultrasonic acetone bath for 20 minutes and dried with compressed blowing air.

Once the specimens were ready, fretting parameters were input via integrated computer software of the fretting wear device. Imposed displacement amplitudes were set to 40 μm and 100 μm under the constant 100 N normal load. The calculated initial Hertz contact stress was 2185 MPa, and contact radius was 296 μm. Linear speed of the oscillating ball was 8 mm/s for all cases, which produces different frequencies for different displacement amplitudes: 50 Hz at 40 μm and 20 Hz at 100 μm. Test durations were 10, 30, and 90 minutes which also produces different number of fretting cycles for both stroke lengths. Each test was repeated at least twice to confirm the consistency of fretting wear results. Fretting parameters are listed in Table 2.

Monitoring the contact responses during fretting is one of the vital requirements to characterize the fretting process. The basic variables such as displacement amplitude and friction coefficient as the ratio of tangential force to normal force (F_t/P) were simultaneously recorded as a function of time by the computer-based data acquisition system. Both

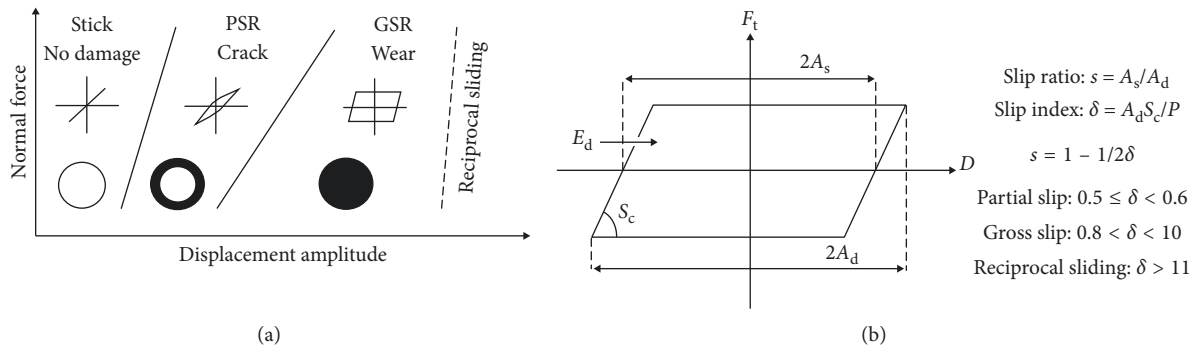

Figure 1: Fretting map for fretting regimes and material response (a), and fretting loop by tangential force vs. displacement amplitude (b) (reproduced from Reference [2]).

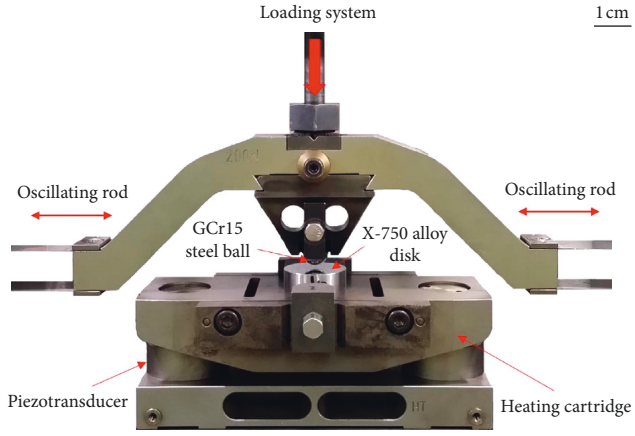

Figure 2: SRV 4 fretting wear test device.

Table 1: Chemical compositions for the frictional pairs (wt.%).

Materials	Elements											
	Ni	Cr	Fe	Ti	Al	Nb + Ta	Mn	Si	S	Cu	C	Co
Inconel X-750	71.6	14.5	5.8	2.6	0.5	0.83	0.62	0.2	0.01	0.01	0.03	0.01
GCr15	0.3	1.46	Bal.	—	—	—	0.36	0.19	0.025	0.06	0.96	—

quantities also can be displayed as a force-displacement (F_t-D) hysteresis loop or fretting loop which is recorded by friction signal analysis module (FSA) for every fretting cycles. Moreover, slip regimes were also confirmed by the universal slip index δ criterion which was mentioned above.

After the samples were collected from fretting tests, they were ultrasonically cleaned again with acetone to remove loose debris from wear scar, and postexperimental analyses were carried out to investigate wear volumes and surface morphologies. Surface topography information was obtained by employing the noncontact 3D optical profiler (Zygo Nexview, AMETEK Inc., USA) to measure the wear volume under the flat surface profile and to generate interactive 3D plots, as well as cross-section profiles of the wear scar. In order to have a high-quality morphology analysis, the worn surfaces were coated with platinum (Pt) in 8.42 nm thickness with 0.11 nm/s sputter rate for 75 seconds. Scanning electron microscopy (SEM) investigations were conducted by TESCAN LYRA3 (Czech Republic) in 2.3e – 2 Pa vacuum chamber pressure and electron beam with 20 kV, to reveal the degradation mechanisms on the worn surface during different fretting regimes. Oxide contents and other chemical compositions on the worn surfaces were detected by using the energy-dispersive X-ray spectroscopy (EDX) embedded analyzer.

Table 2: Fretting test parameters.

Parameters	Values	
Normal load	100 N	
Displacement amplitude	40 μm	100 μm
Frequency	50 Hz	20 Hz
Number of cycles	30000	12000
	90000	36000
	270000	108000
Linear speed	8 mm/s	
Total distance	4.8 m, 14.4 m, 43.2 m	
Relative humidity	50–60%	

3. Results

3.1. Wear Characteristics. The SEM images of wear scars on the lower specimens and superimposed cross-section profiles perpendicular to the fretting direction are shown in Figures 3 and 4 for different amplitudes through the fretting time, respectively. As can be seen, the worn surfaces were in a circular shape for both displacement amplitudes, but with a slight elongation in the direction of fretting for the initial stages of 100 μm amplitude. The fretted surfaces were rough all over, and as the displacement amplitude increases, the size of the worn surface was significantly increased over time (width from 1250 μm to 1750 μm), which indicates full sliding in the whole contact area. In contrast, in the case of 40 μm, the shape of the wear scars was remaining almost same for all fretting tests and very similar to Mindlin's definition, in which the central stick region was formed because of higher contact stresses in the center, while the slight slip was observed in the periphery of the contact due to stick-slip effect [4].

The stick region which was 150 μm in radius (smaller than Hertzian contact radius of 296 μm) after 10 minutes of fretting became narrower twice as much after 90 minutes of fretting test, covered with cracks by the effect of repetitive cyclic stresses.

It is obvious in Figure 4 that the wear scars for 100 μm were wider and deeper than 40 μm. In the initial phases of fretting, the cross-section profiles in PSR demonstrated concave pit due to higher contact pressure, while a bulk of materials was transferred to the contact borders in GSR due to plastic deformation. Later, in Figure 4(c) the wear scars evolved to "W" shape cross section after 90 minutes of fretting for both PSR and GSR. For gross slip conditions, this can be explained with the load-carrying wear debris layer which was mostly generated in the contact annulus rather than in contact center, thus bearing contact pressures near to the contact border [10]. On the other hand, some asperities were popped up at the contact center in PSR, while the peripheral contact region was smooth due to the microslip occurrence. It was evaluated through fretting experiments that the wider asperity areas were observed in the contact center with the smaller imposed displacement amplitudes and the greater normal loads [23].

3D surface mapping and noncontacting wear volume and worn area measurements were obtained by 3D optical surface profiler as illustrated in Figure 5. This process takes the initial step of capturing the millions of data points in the wear scar region with high-precision objective lenses, followed by the selection of worn area to calculate the wear volume under the original flat surface, as depicted in Figures 5(b) and 5(c). Figure 6 gives the information of calculated wear volume, worn area, and wear rate as a function of time for both imposed displacement amplitudes. Wear volumes and worn surface areas have grown dramatically at 100 μm displacement amplitude (i.e., $3.7 \times 10^6\ \mu m^3$ and $9.4 \times 10^4\ \mu m^2$ after 10 min and $13.4 \times 10^6\ \mu m^3$ and $22.6 \times 10^4\ \mu m^2$ after 90 min, respectively), while the progress of wear volume and scar area was very small at 40 μm displacement amplitude, almost negligible values of 0.65 to $0.84 \times 10^6\ \mu m^3$ and 3 to $3.4 \times 10^4\ \mu m^2$ after 10 min and 90 min, respectively.

The wear rate, which is defined to be the volume of material removed per unit sliding distance, $W = V/s$, was decreasing gradually during fretting process for both imposed displacement amplitudes, as shown in Figure 6(c). This process is usually attributed to the running-in or breaking-in effects in the initial fretting periods where the initial wear rate is higher and slowly lowers while the contacting surfaces evolve to their steady-state of wear [24]. Besides, for steel sliding in air, the rise in temperature from frictional heating promotes surface oxidation. Consequently, the wear rate decreases due to the oxide film formation which provides a protective layer against further wear [25, 26].

3.2. Coefficient of Friction. Friction between two counter surfaces was due to the various combined effects of adhesion and abrasion by wear particles and hard asperities deformations. The degree of friction is expressed as a coefficient of friction (μ), which is the ratio of tangential force (F_t) to the normal load (P) and shown in Figure 7 as a function of time. For both imposed displacement amplitudes, rapid growth in COF was observed in the beginning of fretting test in a few seconds, almost jumping to 0.8 value. At 40 μm displacement amplitude, the contact is subjected to partial slip with junction of adhesion and sliding zones; thus, the tangential force remains less than the product of applied normal load and the static friction coefficient. This tendency is described by $F_t < \mu P$, and COF continued in a steady pace for the rest of the test. But at 100 μm, coefficient of friction was decreasing suddenly, dropping to 0.7 for a few ten seconds, followed by gradual increase to the value of 0.9 after about 400 s, and kept at steady-state level. As far as larger relative motion is concerned, this initial rapid rise in COF is believed to be due to the rupture of the *"work-hardening"* or contaminant layer of the surface [16, 18]. The highest wear rate would also be possibly associated with the mass elimination of the contact surface in this period of fretting.

In this experiment, the friction signal was sinusoidal during the entire test without break, as portrayed in Figure 8. The variation of coefficient of friction is plotted during the 600^{th} second for both imposed amplitudes. In Figure 8(a), a pure periodic sine wave was observed in the case of PSR when the amplitude was 40 μm, because the frictional force in the contact interface as a reaction to the imposed amplitude was not enough to cause a full slide. In Figure 8(b), the curve of coefficient of friction at 100 μm was formed as a sine wave with clipped peaks, which indicates the full slide between frictional pairs.

3.3. Fretting Loop. In most of the theoretical and experimental works, the decisions of fretting regime and degradation mechanisms are made based on the *"fretting loop"* which is defined by *"force-displacement"* curve [3, 5, 6, 9–12]. Figure 9 shows the comparative F_t-D curves for partial and gross slip at the onset (after 5 min) and the end (after 90 min) of the fretting test. The partially closed and elliptical curve,

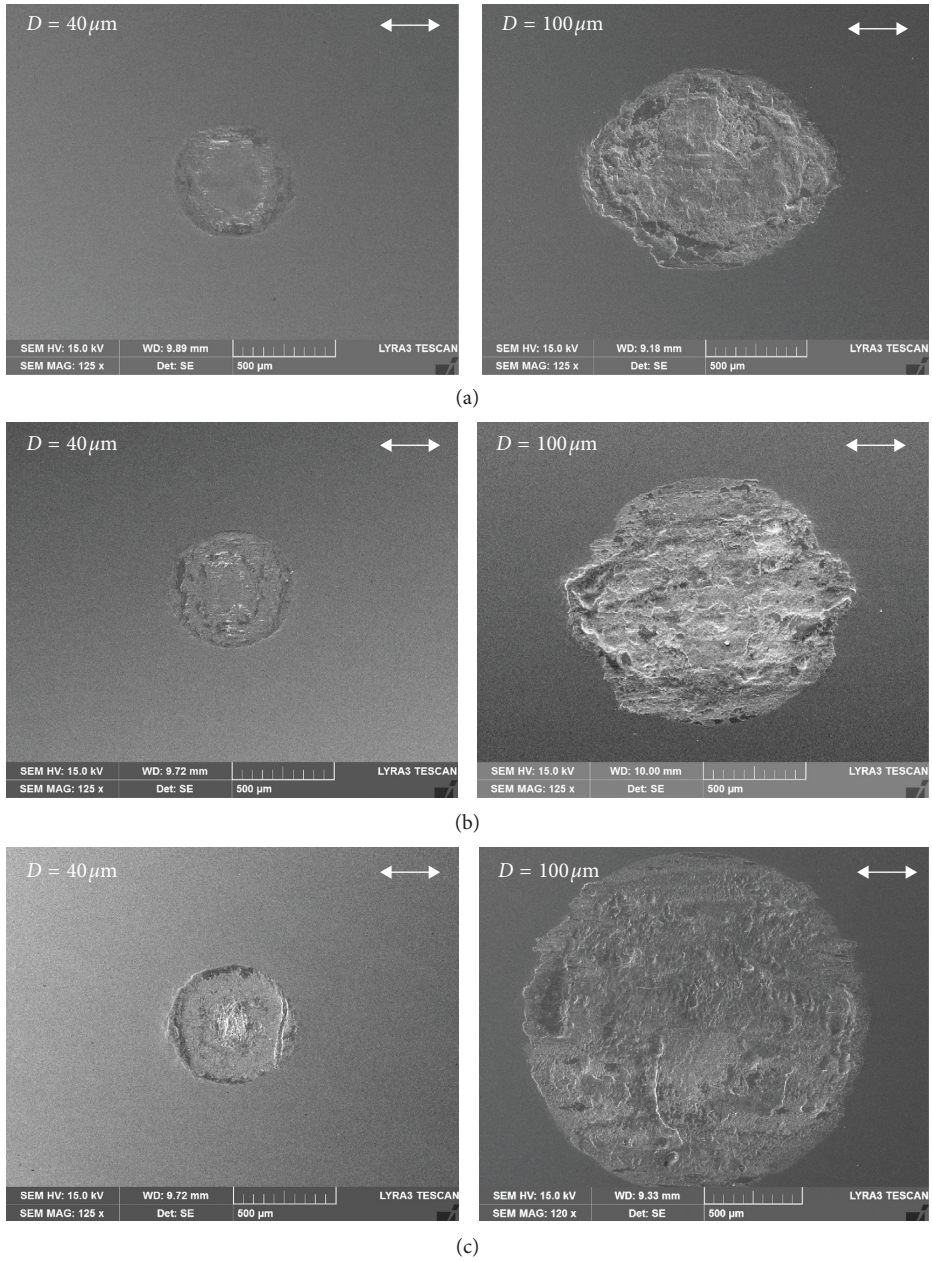

Figure 3: SEM images of worn scars on Inconel X-750 alloy after (a) 10, (b) 30, and (c) 90 minutes of fretting tests. Double arrow indicates fretting direction.

which corresponds to PSR, was obtained for 40 μm in Figure 9(a). However, due to the continuation of cyclic loads, the central mechanical interlocking was reduced and the closed part of the loop was slightly widened after 90 min. This situation is related to the transition from primary elastic to plastic shear form and also due to the limited relative slip and small surface modification at higher normal load. Parallelogram F_t-D curves at 100 μm attributed to GSR where displacement amplitude and thus the area of dissipated energy in the contact interface were greater. In this case, full sliding prevailed in the whole contact interface, resulting in a higher rate of particle detachment, and relative motions were predominantly accommodated by plastic deformation of counter surfaces during the entire fretting process. The fretting loop was kept almost unchanged for the rest of the tests. Besides, fretting regimes according to the slip index criterion were also confirmed which can be calculated as shown in Figure 1(b), and δ found to be 0.56 for PSR, while $\delta = 1.06$ for GSR, both cases satisfying the transition restrictions for slip index.

3.4. Worn Scar Morphology. The consequences of these mentioned frictional effects on the Inconel X-750 alloy and GCr15 steel ball specimens were investigated for partial and gross slip conditions by observing SEM morphologies. Figure 10 shows the damage evolutions on the flat material at the stick and slip domains when the displacement amplitude

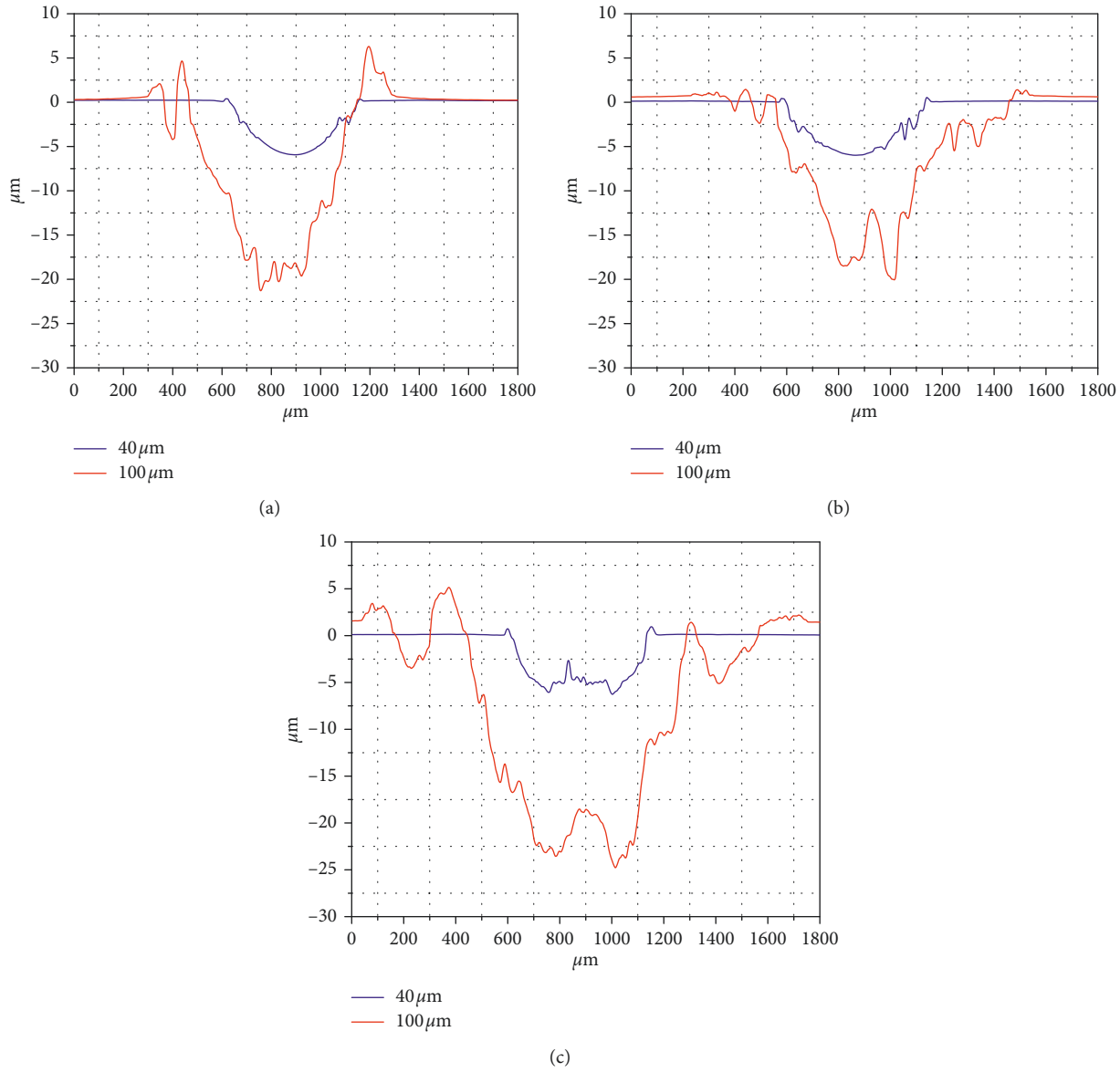

Figure 4: Superimposed cross-section profiles of wear scars perpendicular to the fretting direction through fretting time. (a) After 10 minutes. (b) After 30 minutes. (c) After 90 minutes.

at 40 μm. It was found that PSR was dominant in the contact area, with the mechanical interlocking of the asperities in the contact center and adhered fretting scars due to the microslips in the contact annulus. However, the degree of these degradation mechanisms was changing over the number of fretting cycles. For instance, Figure 10(a) shows the fretting scars after 10 min with limited material damage: the stick domain was smooth and surrounded by tiny pits due to the ratcheting effect. In the later stages of fretting cycles (9×10^4), many microcracks surrounded the shrinking stick area while the long crack perpendicular to the fretting direction appeared in the contact border which looks like in the stage of delamination process (Figure 10(b)). Furthermore, the sign of thick layer of material removal by harder GCr15 ball was observed in the slip region. The contact center was slowly worn out during the further fretting test by overstressing, and the wear mode was completely changed after a considerable number of cycles (2.7×10^5) as shown in Figure 10(c), where the stick domain was totally rough and covered with radial microcracks which were induced by fretting fatigue. On the other hand, the longer crack was detected along the far end of the contact which was partially filled with wear debris. The slip region also has been changed since the previous condition where some layer of the annulus was transferred by opposite surface, and this time, the remaining layers of the contact annulus was removed by further cyclic stress which was assumed to be the exhaustion of ductility due to the plasticity accumulation by ratcheting.

SEM morphologies in Figure 11 shows that the whole contact interface was in full slide at 100 μm, and degradation mechanisms were associated with adhesion, abrasion, delamination, oxidation, and plastic deformation, as well as

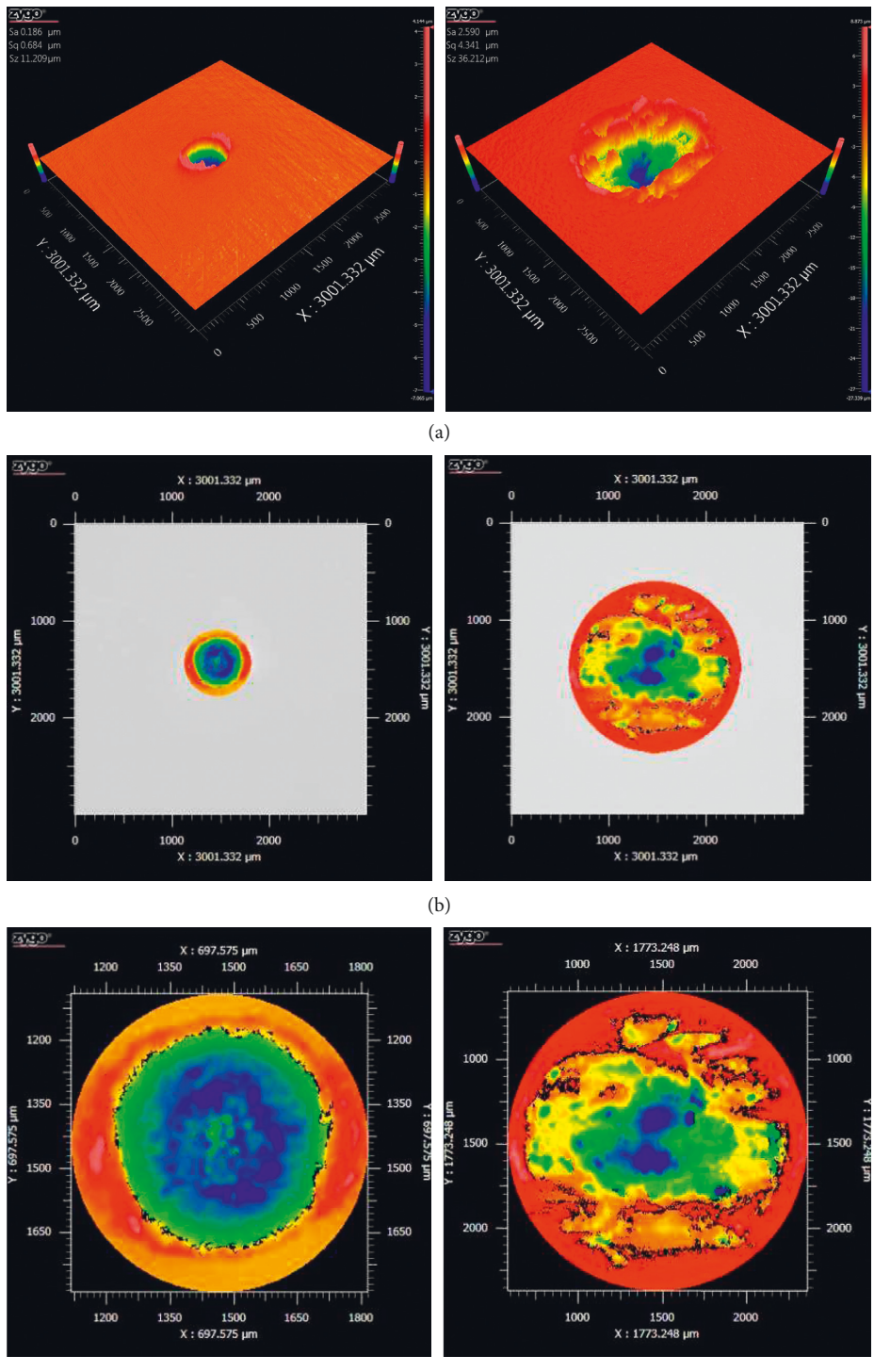

Figure 5: Surface topographies of worn scars for (a) 40 μm (left) and 100 μm (right) after 90 minutes of fretting test; (b) corresponding preprocessed input area; and (c) selected worn area to calculate the wear volume.

third-body flow between contact surfaces. Red-brown oxidized powders were ejected from contact surfaces during the fretting process which can serve as abrasive particles prior to their expulsion. For example, Figure 11(a) shows the wear mode onset of the fretting process in the contact center, where plowing grooves parallel to the sliding direction, was formed due to the larger relative motion by abrasive particles, followed by plastic shearing so that thick layers of X-750 alloy were peeled off by adhesion. Adhesive wear is often occurred at the onset of fretting when friction pairs come into contact, followed by plastic shearing that plucks off the ends of the softer asperities. This phenomenon is also

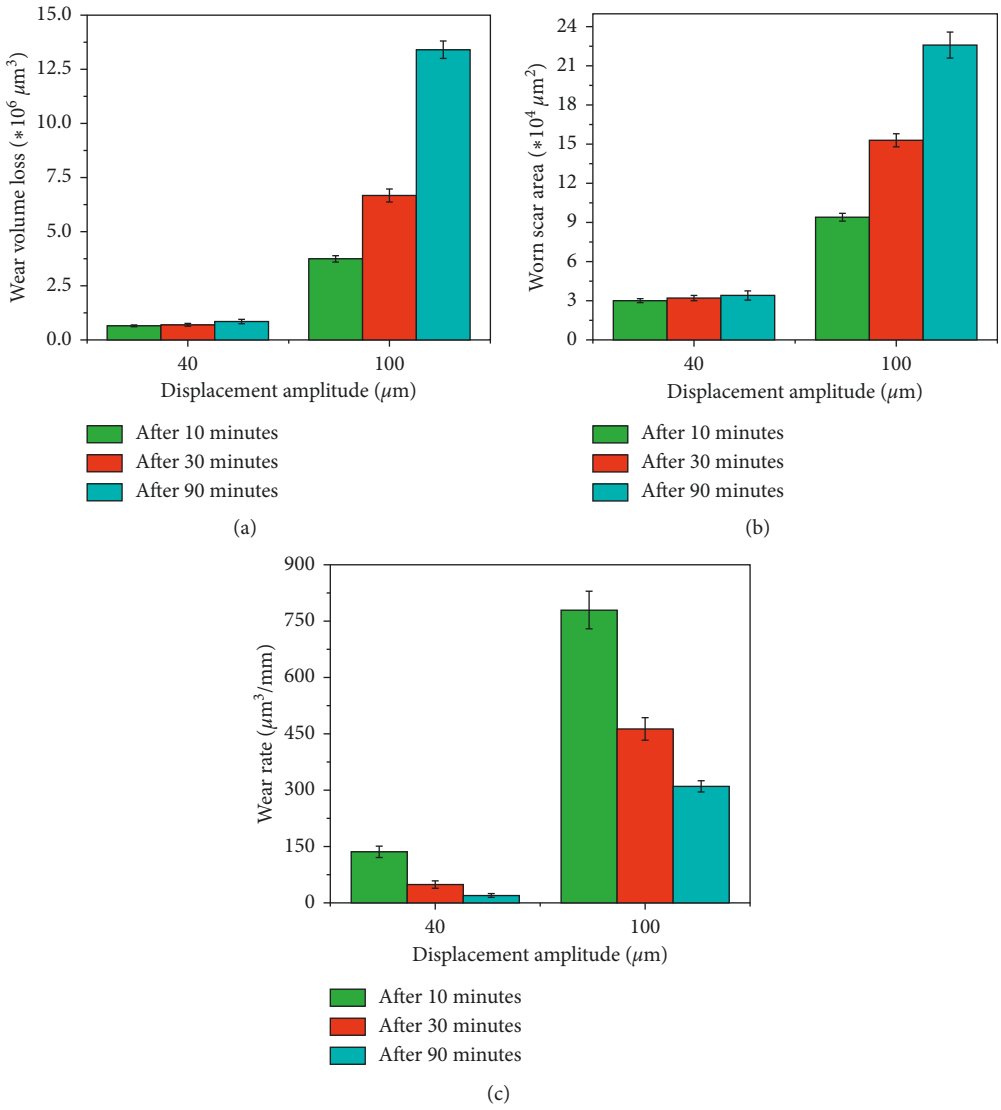

Figure 6: Calculated wear volumes (a), worn scar areas (b), and wear rates (c) after different time of fretting.

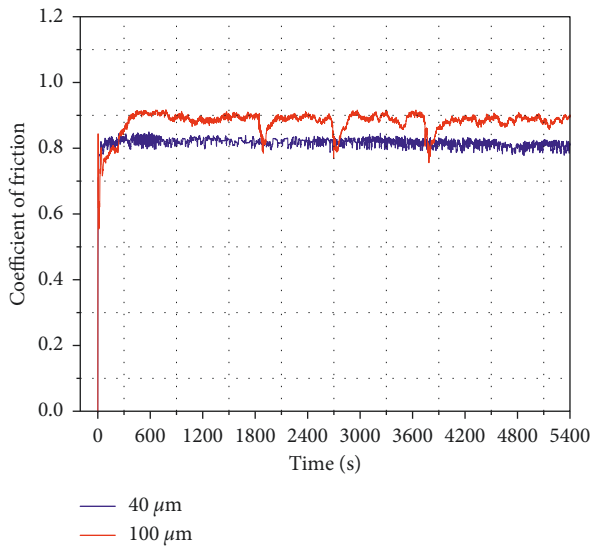

Figure 7: Coefficient of friction for contact pairs as a function of time.

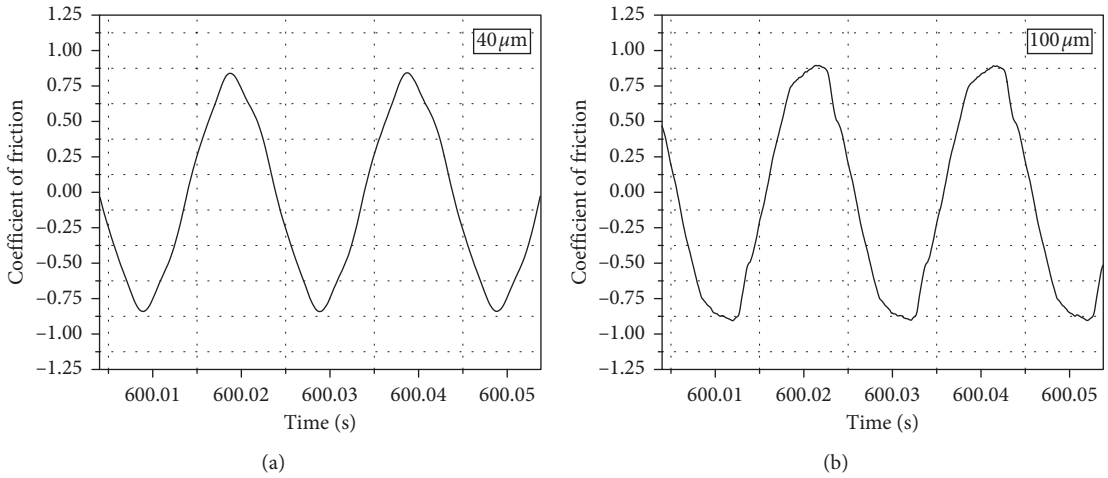

Figure 8: Sinusoidal coefficient of frictions during 600 s fretting time for (a) 40 μm and (b) 100 μm.

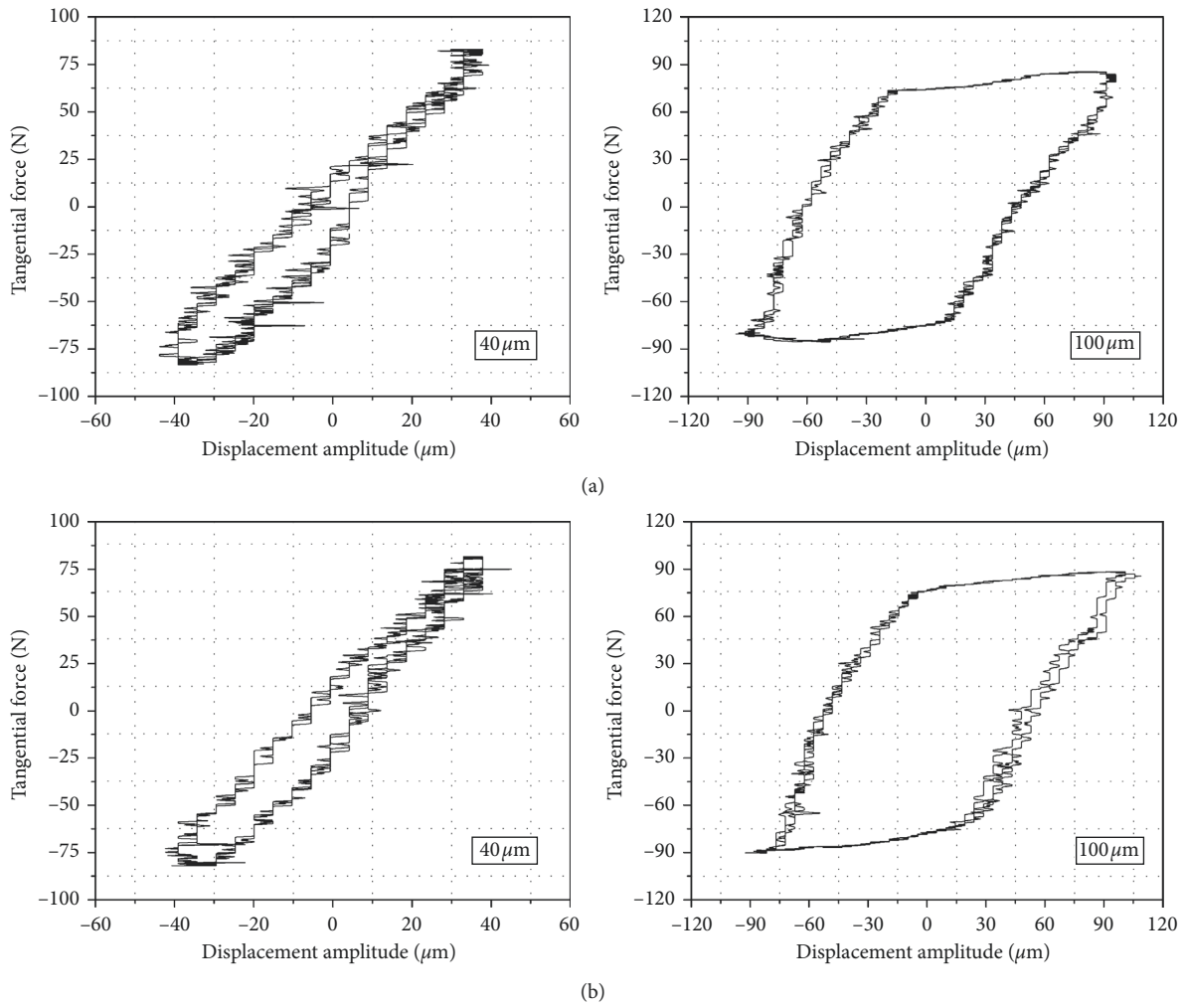

Figure 9: Evolution of fretting loops for 40 μm and 100 μm after (a) 5 and (b) 90 minutes of fretting.

attributed to galling and scuffing [13]. Figure 11(b) shows the magnified image in Figure 11(a) that the crack propagations were prevented by particle detachment and started to spall, eventually becoming loose wear debris. Fretted surfaces were rough owing to the plastic deformation and ploughing effects, and in some cases, surface roughening would provide

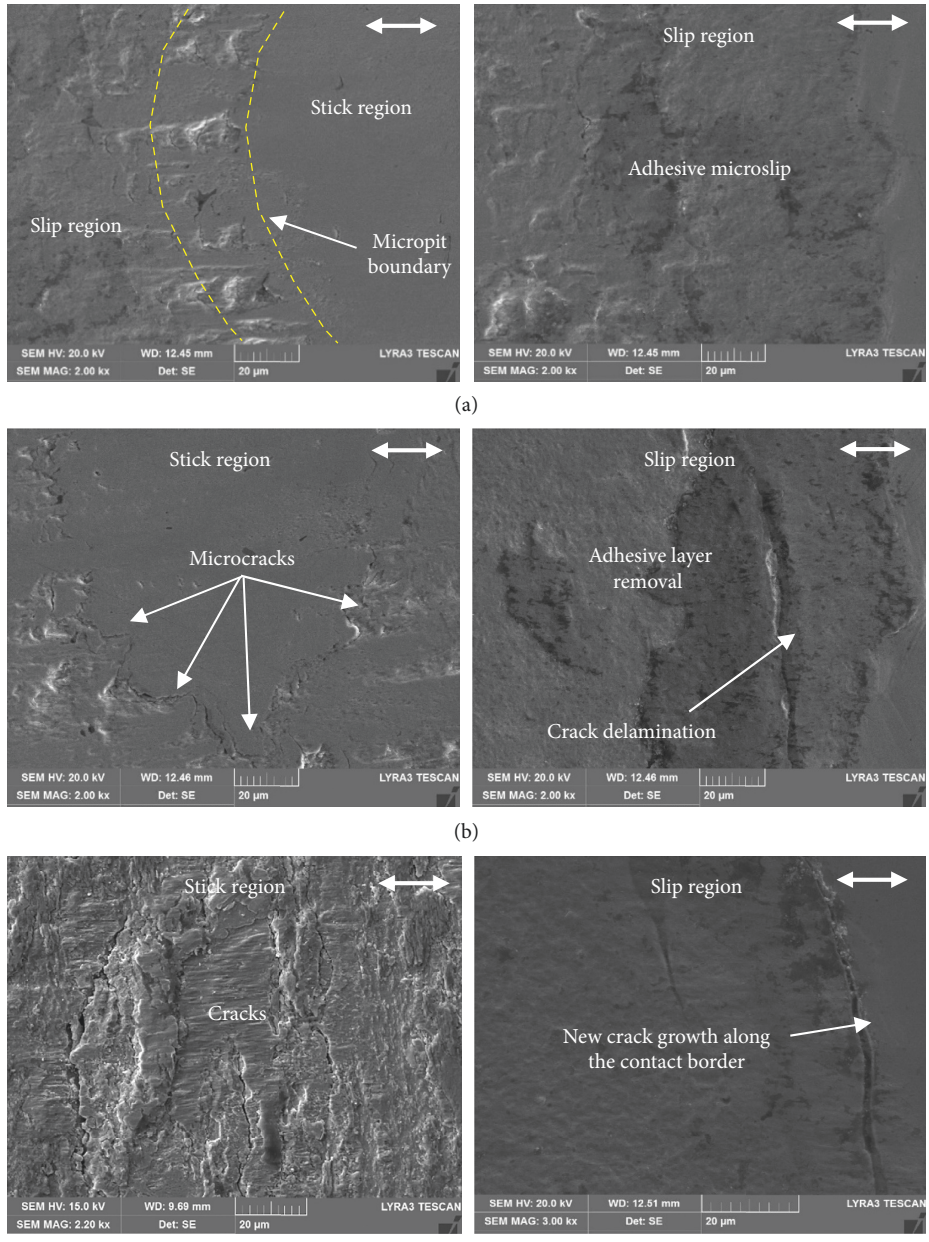

Figure 10: SEM micrographs of Inconel X-750 wear scars during PSR: (a) after 10 minutes, (b) after 30 minutes, and (c) after 90 minutes of fretting. Displacement amplitude is 40 μm. Double arrows represent fretting direction.

escape channels for wear debris. As the fretting test continued, the contact interfaces were slowly accommodated by the plastic flow and further loading promoted the growth of subsurface cracks that parallel to the surface. When these cracks finally extended out to the free surface, thin platelet-like wear particles delaminated, as shown in Figures 11(c) and 11(d). In the same time, when the delamination was occurring mostly in the contact center, plastic flow of the contacting surfaces in the periphery, and third-body flow close to the contact border were observed in Figures 11(e) and 11(f), respectively. Moreover, as temperature increases because of frictional heating during GSR, oxidation of the wear particles becomes more ubiquitous, and as a consequence, thicker, more continuous oxide layer will be generated. The greater contact temperature at this condition also causes plastic flow of the oxide film, leading to more severe oxidational wear [19].

Figure 12 shows the SEM images of wear scars and corresponding 3D surface topographies of the steel balls oscillated at 40 μm and 100 μm after 90 minutes of fretting. Both wear scars were in a circular shape. The worn surface area, which was oscillated at 40 μm, also contains the stick domain in the contact center and slip domain at the periphery, as shown in Figure 12(a). However, it is clear from the picture that a bulk of oxidized X-750 alloy surface layer in black was adhered to the half annulus of the contact which

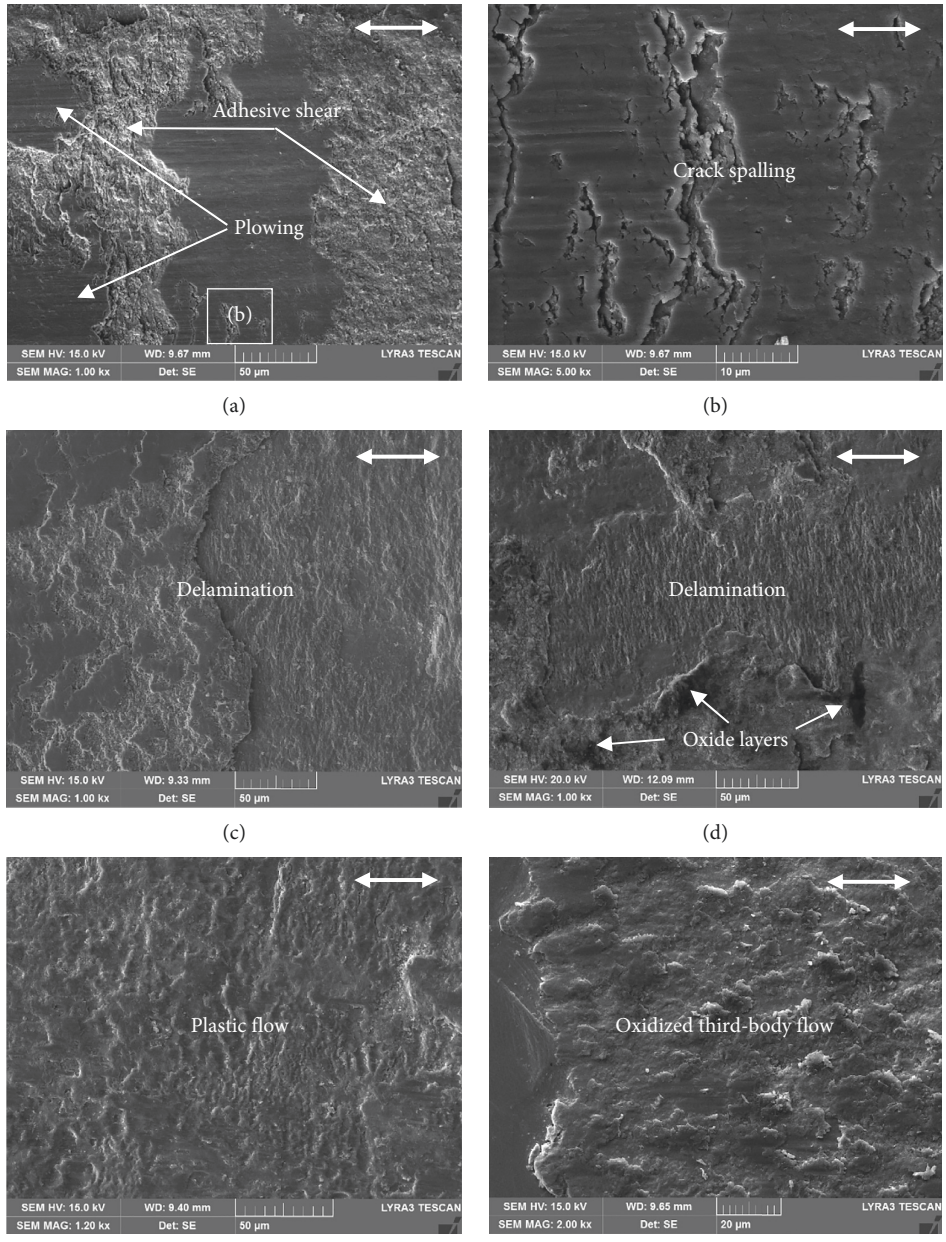

Figure 11: SEM micrographs of Inconel X-750 wear scars during GSR: (a) mixed abrasive and adhesive wear at the onset of fretting process, (b) spalling of cracks, (c, d) delamination, (e) plastic flow, and (f) third-body flow near contact border. Displacement amplitude is 100 μm. Double arrows represent fretting direction.

was believed to be plucked off by harder GCr15 ball surface during fretting induced by fatigue. According to the wear scar in Figure 12(b), GSR was dominant at 100 μm with the sign of abrasion and small amount of transferred materials on the worn surface. Figure 13 shows the EDX spectrum information for the marked spots in Figure 12 on the wear scar areas. Oxide content was very low (1.46 wt.%) in the stick region due to the constriction of the relative motion, while microslip region was reacting with the oxygen in a small amount. On the other hand, the highly concentrated oxygen content (29 wt.%) was detected on the transferred flat material in Figure 13(c). However, the oxidation process on the worn steel surface was faster during GSR rather than PSR (Figure 13(d)).

4. Discussion

The fretting wear process in an ambient temperature is often determined by the contact geometry, the oxidation process, and the subsequent third-body behavior in the contact interface, which significantly affect the friction and wear properties in dry air [11, 16, 27]. Wear properties, such as, volume, scar area, and depth, were considerably lower during PSR than GSR as shown in Figures 3–6, because of

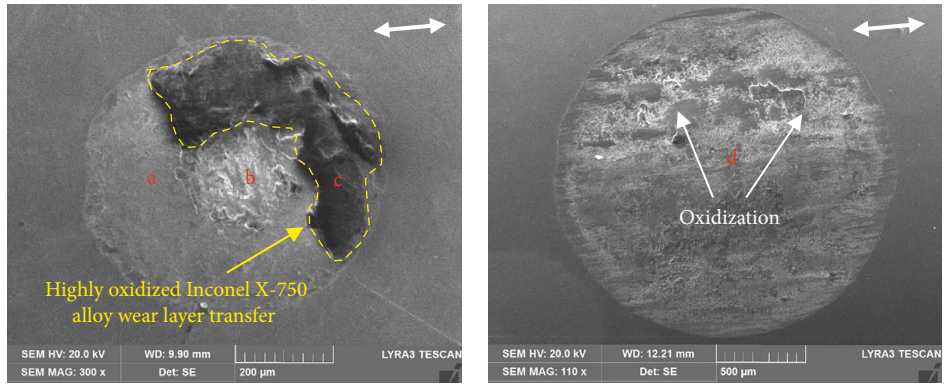

(a) (b)

Figure 12: SEM morphologies of GCr15 steel ball worn scars oscillating at (a) 40 μm and (b) 100 μm. Fretting time is 90 minutes. Double arrows represent fretting direction.

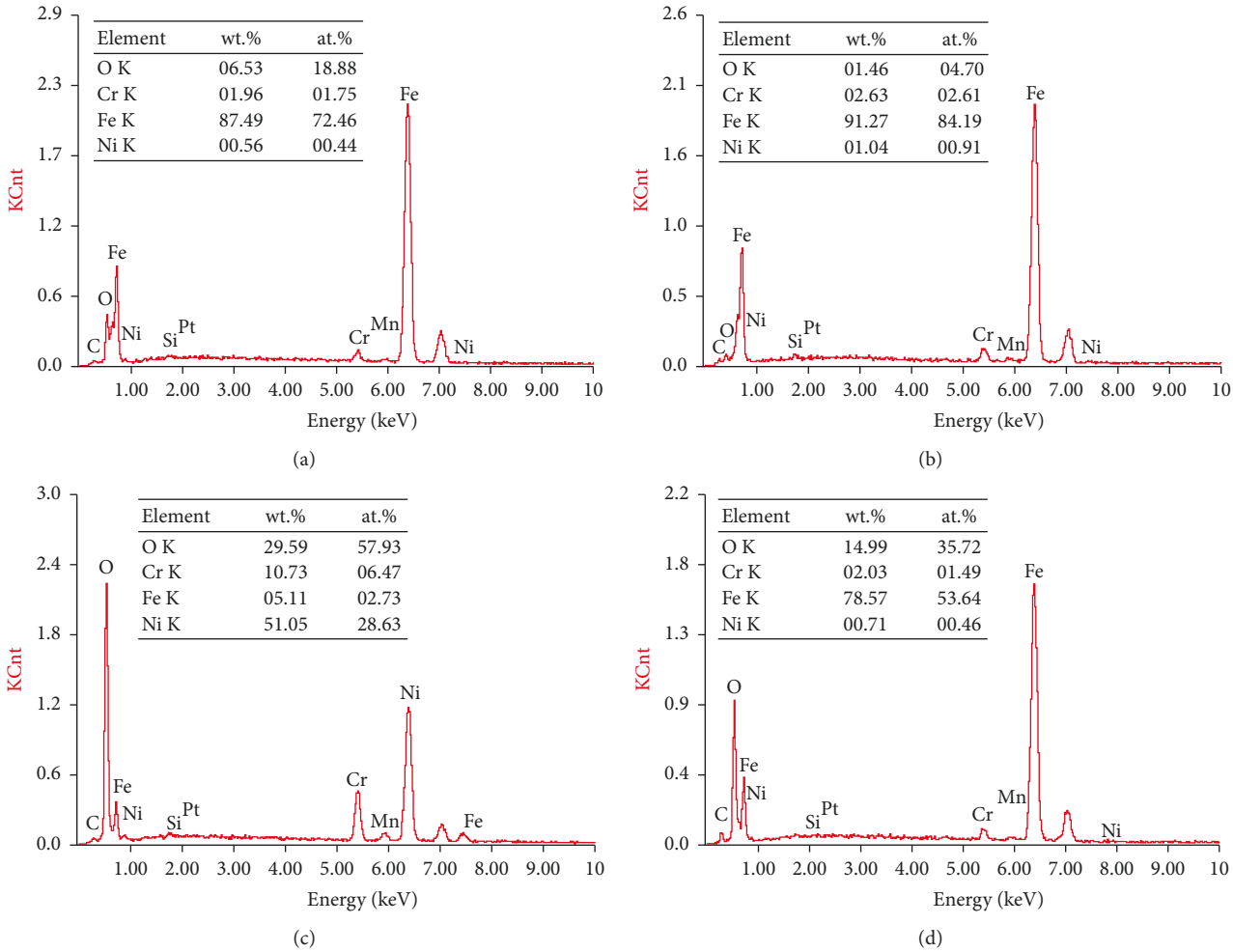

Figure 13: EDX spectroscopy analysis for worn surfaces at marked spots in Figure 12.

the small imposed contact area compared to the scale of the normal load applied. Yet, the wear rate was maximum in the running-in period for both cases, decreasing gradually with fretting time in Figure 6(c), typically due to the formation of the oxide layer (also *"glaze"* layer) on the worn surface which can enhance the load-carrying capacity, avoiding further wear [28]. During the partial and gross slip conditions, the friction is the outcome of the direct interlocking of the surface asperities and the trapped oxide debris behavior in the contact interface, respectively. In Figure 7, the COF

during PSR was always lower with no apparent fluctuation during the steady-stage level due to the minimum tangential force between the contact interfaces, where the central zones were mechanically interlocked. In this case, the higher normal load triggers the traction coefficient where the critical total sliding shear force is always higher than the tangential force [5, 11]. However, in GSR, the highest peak of friction occurred prior to the fluctuating steady-stage level, mainly due to the strong plastic deformation of work-hardened layer of the contacting surfaces [23, 29]. On the other hand, the fluctuations in COF are attributed to the modifications in the contact interface which are linked to the third-body rheology, i.e, wear debris formation and its entrapment and ejection from the contact zone [27].

The fretting loops generated by F_t-D curves in Figure 9 are good indicators to show the slip condition at any moment. The area enclosed by the curves is the measure of dissipated energy produced by friction [10, 30]. The friction work performed provides a more representative explanation of the surface damage. Usually, it has been noticed that the wear volume, V, is proportional to the energy dissipated, E_d, in the contact and described as $V = \alpha \times \sum E_d$, where α is the friction energy wear coefficient [6]. The degree of slope, S_c, can be considered as wear characteristics of the sliding conditions and materials. Besides, the unified slip index approach also offers the knowledge of fretting conditions and considered as an appropriate means for estimating fretting wear problems. In accordance with the terms of slip index, when the slip ratio $s \longrightarrow 0$, the contacts are in stick, and as the slip ratio approaches to 1, partial slip, and then gross slip prevail [2]. The partial slip contacts in small displacements induce cyclic stresses, which favor crack nucleation and propagation, but the loading condition is nondissipative with limited surface damage at the periphery as shown in Figure 10. However, the friction dissipation in GSR, correlated with the plastic flow, delamination, and oxidation wear mechanisms, causes a large amount of surface damage by extending the contact area and reducing the contact pressure profile (Figure 11).

The main damage mechanisms, i.e., cracking (fretting induced by fatigue) and material loss (fretting induced by wear), are often appear as a competing process which was extensively explored during the last decade [1, 3, 5, 6, 31–34]. For instance, the material loss during GSR can eliminate small cracks or fill up the opening of a deep crack and accommodate the main portion of the imposed displacement; as a consequence, it strongly reduces the slip amplitude and then the debris formation. In fact, the debris ejection has great impact on the third-body establishment: if it is trapped between the contacts, the degradation process can be suppressed and the most of the velocity difference between the friction pairs would be completely accommodated in a dissipative manner by the powder bed [33, 34]. As for cracking, the effects of frictional force and the contact load are huge on the crack initiation and growth during fretting fatigue, where the frictional force triggers the crack initiation, while the contact load disrupts the crack growth during the propagation period [37]. Meanwhile, it is reported that the cracks on the worn scar surface nucleated and propagated along the direction of 30–50° to the surface interior which was in the range of calculated maximum shear stress angle [18].

SEM morphology in Figure 12(a) shows the interesting wear phenomenon, where the thick layer of Inconel X-750 alloy was stuck to the worn surface of the oscillating ball due to the adhesive microslip. In return, with the further fretting, the material transferred to the surface of GCr14 ball has the highest possibility to transfer back to the previous worn surface of Inconel X-750 alloy [8]. Besides, the transferred wear layer was highly oxidized compared to the stick and slip regions of the steel ball as shown in Figure 13. The debris detached from the contact pairs is essentially composed of nonmagnetic single component oxides, e.g., Fe_2O_3, NiO, and Cr_2O_3, or more complex oxides, e.g., $NiCr_2O_4$ and $NiFe_2O_4$ [38]. However, the oxidization process was rapid on the worn surface of the steel ball during GSR, which is because of more mechanical energy being converted to the thermal heat, and it is believed that the frictional heat during GSR was higher than in PSR [19].

5. Conclusion

The main purpose of this study was to explore the degradation evolutions of Inconel X-750 co-acted with GCr15 steel ball through the dry fretting tests and observations/analyses by using 3D surface profiler, SEM, and EDX. According to the results, the conclusions can be drawn as follows:

(i) The degradation mechanisms of Inconel X-750 were totally dependent on the fretting regimes and varied with the fretting time.

(ii) The wear volume and wear depth were very low in PSR, and wear mechanisms were associated with the deformations, adhesion, and fatigue crack. The microcracks were present around the stick domain in 3×10^4 cycle, and the radial cracks fully covered the contact center above 10^5 cycle, along with the bigger crack in the contact border. The large layer of ductile X-750 alloy was transferred to the wear surface of the steel ball due to the exhaustion by highly concentrated cyclic loading during the later stages of fretting.

(iii) In GSR, the degradation mechanisms were as follows: (1) adhesive wear (galling and scuffing); (2) abrasive wear by third-body particle, which is a mechanical removal process; (3) delamination, which is influenced by the material fatigue in the shallow subsurface layer; and (4) oxidation of debris particles and surface layer due to the higher frictional heat, which can enhance the load-carrying capacity, as well as reduce the wear rate in the later stages of fretting process.

(iv) The dependence of fretting time was negligible during PSR in respect of wear properties, such as wear volume, scar area, and depth. However, it has a great impact to evolve the degradation mechanisms

from asperity deformation to the crack initiation and propagation, which is a critical damage during PSR. On the other hand, the wear volume and scar area were increased significantly by time during GSR, but the degradation evolutions were combined and repeated with the mentioned wear mechanisms in a whole fretting process.

Data Availability

The data used to support the findings of this study are available from the corresponding author upon request.

Conflicts of Interest

The authors declare that there are no conflicts of interest regarding the publication of this paper.

Acknowledgments

The first author would like to acknowledge the scholarship support from China Scholarship Council (CSC). This work was supported by the Aeronautical Science Fund of China (Grant no. 20164058002), National Natural Science Foundation of China (Grant No.51735006), and Tsinghua University Initiative Scientific Research Program.

References

[1] R. B. Waterhouse, "Fretting wear," *Wear*, vol. 100, no. 1–3, pp. 107–118, 1984.

[2] M. Varenberg, I. Etsion, and G. Halperin, "Slip index: a new unified approach to fretting," *Tribology Letters*, vol. 17, no. 3, pp. 569–573, 2004.

[3] O. Vingsbo and S. Söderberg, "On fretting maps," *Wear*, vol. 126, no. 2, pp. 131–147, 1988.

[4] R. D. Mindlin and H. Deresiewiez, "Elastic spheres in contact under varying oblique forces," *Journal of Applied Mechanics*, vol. 20, pp. 327–344, 1953.

[5] Z. R. Zhou and L. Vincent, "Mixed fretting regime," *Wear*, vol. 181–183, pp. 531–536, 1995.

[6] S. Fouvry, P. Kapsa, and L. Vincent, "Quantification of fretting damage," *Wear*, vol. 200, no. 1-2, pp. 186–205, 1996.

[7] J. Yu, L. Qian, B. Yu, and Z. Zhou, "Nanofretting behavior of monocrystalline silicon (100) against SiO_2 microsphere in vacuum," *Tribology Letters*, vol. 34, no. 1, pp. 31–40, 2009.

[8] H. Mohrbacher, J. P. Celis, and J. R. Roos, "Laboratory testing of displacement and load induced fretting," *Tribology International*, vol. 28, no. 5, pp. 269–278, 1995.

[9] Z. R. Zhou, S. Fayeulle, and L. Vincent, "Cracking behaviour of various aluminium alloys during fretting wear," *Wear*, vol. 155, no. 2, pp. 317–330, 1992.

[10] S. Fouvry, P. Kapsa, H. Zahouani, and L. Vincent, "Wear analysis in fretting of hard coatings through a dissipated energy concept," *Wear*, vol. 203-204, pp. 393–403, 1997.

[11] J. Li and Y. H. Lu, "Effects of displacement amplitude on fretting wear behaviors and mechanism of Inconel 600 alloy," *Wear*, vol. 304, no. 1-2, pp. 223–230, 2013.

[12] G. B. Stachowiak and G. W. Stachowiak, "Fretting wear and friction behaviour of engineering ceramics," *Wear*, vol. 190, no. 2, pp. 212–218, 1995.

[13] B. Bhushan and B. K. Gupta, *Handbook of Tribology: Materials, Coatings, and Surface Treatments*, McGraw-Hill, New York, NY, USA, 1991.

[14] H. Y. Zhang, Y. H. Lu, M. Ma, and J. Li, "Effect of precipitated carbides on the fretting wear behavior of Inconel 600 alloy," *Wear*, vol. 315, no. 1-2, pp. 58–67, 2014.

[15] X. Mi, W. X. Wang, X. M. Xiong et al., "Investigation of fretting wear behavior of Inconel 690 alloy in tube/plate contact configuration," *Wear*, vol. 328-329, pp. 582–590, 2015.

[16] L. Jie, L. Yonghao, Z. Haoyang, and L. Xin, "Effect of grain size and hardness on fretting wear behavior of inconel 600 alloys," *Tribology International*, vol. 81, pp. 215–222, 2015.

[17] L. Xin, B. B. Yang, Z. H. Wang, J. Li, Y. H. Lu, and T. Shoji, "Microstructural evolution of subsurface on inconel 690TT alloy subjected to fretting wear at elevated temperature," *Materials & Design*, vol. 104, pp. 152–161, 2016.

[18] J. Li, B. B. Yang, Y. H. Lu, L. Xin, Z. H. Wang, and T. Shoji, "The degradation mechanism of inconel 690TT induced by fretting wear in air," *Tribology International*, vol. 116, pp. 147–154, 2017.

[19] G. Xianglong, L. Ping, T. Lichen et al., "Effects of sliding amplitude and normal load on the fretting wear behavior of alloy 690 tube exposed to high temperature water," *Tribology International*, vol. 116, pp. 155–163, 2017.

[20] Special Metals, INCONEL alloy X-750 Data Sheet, 2004, Publication No. SMC-067, http://www.specialmetals.com.

[21] C. Marsh, S. Depinoy, and D. Kaoumi, "Effect of heat treatment on the temperature dependence of the fracture behavior of X-750 alloy," *Materials Science and Engineering: A*, vol. 677, pp. 474–484, 2016.

[22] D. Wenbo, S. Yanhua, D. Chunhua, and Y. Lie, "Structural stiffness of X-750 alloy bump foil strips for compliant foil bearings with different heat treatments," *Journal of Tribology*, vol. 138, no. 3, article 031702, 2016.

[23] G. X. Chen and Z. R. Zhou, "Study on transition between fretting and reciprocating sliding wear," *Wear*, vol. 250, no. 1–12, pp. 665–672, 2001.

[24] J. F. Archard, "Contact and rubbing of flat surfaces," *Journal of Applied Physics*, vol. 24, no. 8, pp. 981–988, 1953.

[25] S. C. Lim, M. F. Ashby, and J. H. Brunton, "Wear-rate transitions and their relationship to wear mechanisms," *Acta Metallurgica*, vol. 35, no. 6, pp. 1343–1348, 1987.

[26] S. C. Lim, "Recent developments in wear-mechanism maps," *Tribology International*, vol. 31, no. 1–3, pp. 87–97, 1998.

[27] X. Long, W. Zihao, L. Jie, Y. Lu, and T. Shoji, "Microstructural characterization of subsurface caused by fretting wear of inconel 690TT alloy," *Material Characteristics*, vol. 115, pp. 32–38, 2016.

[28] R. Rybiak, S. Fouvry, and B. Bonnet, "Fretting wear of stainless steels under variable temperature conditions: introduction of a "composite" wear law," *Wear*, vol. 268, no. 3-4, pp. 413–423, 2010.

[29] J. F. Zheng, J. Luo, J. L. Mo, J. F. Peng, X. S. Jin, and M. H. Zhu, "Fretting wear behaviors of a railway axle steel," *Tribology International*, vol. 43, no. 5-6, pp. 906–911, 2010.

[30] K. V. Virendra, N. Hamza, S. S. R. Ganesh, H. Murthy, A. N. Majila, and D. C. Fernando, "Effect of contact pressure and stress ratio on the fretting fatigue behaviour of Ti-6Al-4V," *Material Science and Engineering: A*, vol. 707, pp. 647–656, 2017.

[31] J. J. Madge, S. B. Leen, and P. H. Shipway, "The critical role of fretting wear in the analysis of fretting fatigue," *Wear*, vol. 263, no. 1–6, pp. 542–551, 2007.

[32] P. Arnaud, S. Fouvry, and S. Garcin, "Wear rate impact on Ti-6Al-4V fretting crack risk: experimental and numerical comparison between cylinder/plane and punch/plane contact geometries," *Tribology International*, vol. 108, pp. 32–47, 2017.
[33] M. H. Zhu and Z. R. Zhou, "On the mechanisms of various fretting wear modes," *Tribology International*, vol. 44, no. 11, pp. 1378–1388, 2011.
[34] W. S. Gwidon, *Wear-Materials, Mechanisms and Practice*, John Wiley and Sons, Ltd., Hoboken, NJ, USA, 2005.
[35] M. Godet and Y. Berthier, "Continuity and dry friction: an osborne reynolds approach," *Tribology Series*, vol. 11, pp. 653–661, 1987.
[36] Y. Berthier, L. Vincent, and M. Godet, "Velocity accommodation in fretting," *Wear*, vol. 125, no. 1-2, pp. 25–38, 1988.
[37] F. C. Castro, J. A. Araújo, E. N. Mamiya, and N. Zouain, "A fatigue endurance criterion in two stages with application to fretting contact," *Tribology International*, vol. 42, no. 9, pp. 1297–1303, 2009.
[38] G. C. Wood and B. Chattopadhyay, "Transient oxidation of Ni-base alloys," *Corrosion Science*, vol. 10, no. 7, pp. 471–480, 1970.